

# RSC Advances



This is an *Accepted Manuscript*, which has been through the Royal Society of Chemistry peer review process and has been accepted for publication.

*Accepted Manuscripts* are published online shortly after acceptance, before technical editing, formatting and proof reading. Using this free service, authors can make their results available to the community, in citable form, before we publish the edited article. This *Accepted Manuscript* will be replaced by the edited, formatted and paginated article as soon as this is available.

You can find more information about *Accepted Manuscripts* in the [Information for Authors](#).

Please note that technical editing may introduce minor changes to the text and/or graphics, which may alter content. The journal's standard [Terms & Conditions](#) and the [Ethical guidelines](#) still apply. In no event shall the Royal Society of Chemistry be held responsible for any errors or omissions in this *Accepted Manuscript* or any consequences arising from the use of any information it contains.

## Hierarchical $\text{WO}_3$ nanostructured thin films with enhanced electrochromic performance for switchable smart windows†

S. Poongodi<sup>a</sup>, P. Suresh Kumar<sup>b</sup>, Yoshitake Masuda<sup>c</sup>, D. Mangalaraj<sup>a\*</sup>, N. Ponpandian<sup>a</sup>,

C. Viswanathan<sup>a</sup>, Seeram Ramakrishna<sup>d</sup>

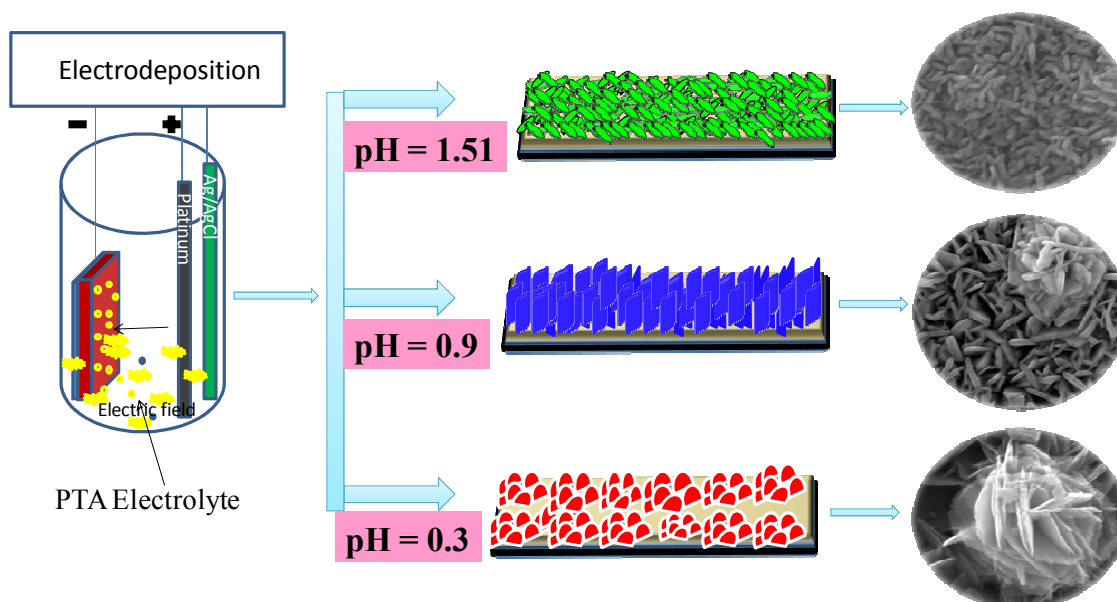
<sup>a</sup> Department of Nanoscience and Technology, Bharathiar University, Coimbatore 641 046, India.

<sup>b</sup> Environmental & Water Technology, Centre of Innovation, Ngee Ann Polytechnic, Singapore 599489, Singapore.

<sup>c</sup> National Institute of Advanced Industrial Science and Technology (AIST), 2266-98 Anagahora, Shismoshidami, Moriyama-ku, Nagoya 436-8560, Japan.

<sup>d</sup> Center for Nanofibers and Nanotechnology, Department of Mechanical Engineering, National University of Singapore, Singapore 117576.

### Graphical Abstract





Journal Name

ARTICLE

## Synthesis of Hierarchical WO<sub>3</sub> nanostructured thin films with enhanced electrochromic performance for switchable smart windows†

Received 00th January 20xx,  
Accepted 00th January 20xx

DOI: 10.1039/x0xx00000x

[www.rsc.org/](http://www.rsc.org/)

S. Poongodi<sup>a</sup>, P. Suresh Kumar<sup>b</sup>, Yoshitake Masuda<sup>c</sup>, D. Mangalaraj<sup>a\*</sup>, N. Ponpandian<sup>a</sup>, C. Viswanathan<sup>a</sup>, Seeram Ramakrishna<sup>d</sup>

In our present work, hierarchical WO<sub>3</sub> nanostructured thin films were successfully synthesized over pre-deposited seed layered FTO substrates through electrodeposition method. By adjusting the pH values of the electrolyte, three different morphologies such as nanospindles (W1), nanoplatelets (W2), and hierarchical flower (W3) like nanoarray film have been obtained. The structural, surface, compositional and optical performance of the WO<sub>3</sub> nanostructured thin films were characterized by XRD, FESEM, AFM, XPS, UV-VIS and detailed electrochromic functionality was performed by cyclic voltammogram (CV) at different applied potentials. Among the three nanostructured thin films electrodes (W1, W2, W3), W3 exhibits excellent larger optical contrast (79.90% at 550 nm), faster switching response time ( $t_b = 3.82s$  and  $t_c = 5.05s$ ), and superior coloration efficiency ( $172.08 \text{ cm}^2 \text{ C}^{-1}$ ) with stability over 2000 cycles. The synthesized WO<sub>3</sub> electrode (W3) with flower morphology shows excellent reversibility of around 94.11% than other nanostructure (W1 and W2) due to its enhanced crystallinity and high porosity. Our results suggests that flower like WO<sub>3</sub> nanostructured thin film electrode will have a great impact on the large scale production and makes the material a promising candidate for fabrication of efficient electrochromic devices.

### 1. Introduction

In the recent decades, tungsten trioxide has received great attention because of its commercial applications such as in smart windows, display devices, eyewear, mirrors, mobile phones, smart cards, price labels, photocatalysis, solar cells and hydrogen generation.<sup>1,2</sup> Numerous transition metal oxides have been exploited as inorganic electrode materials for the fabrication of electrochromic devices. Among the transition metal oxides, tungsten trioxide (WO<sub>3</sub>) has been recognized as one of the versatile inorganic cathode electrode materials for electrochromic applications owing to its distinct electrochromic response, high cyclic stability, high coloration efficiency and intercalation properties.<sup>2,3</sup> Electrochromism refers to the reversible alteration of optical modulation on application of external voltage. This can be attributed to the intercalation/de-intercalation of ions (such as H<sup>+</sup>, Na<sup>+</sup>, etc.)

into/from the host metal oxide lattice. Moreover, WO<sub>3</sub> based Electrochromic Displays (ECD) exhibit low power consumption, high contrast ratio, good memory effects and chemical stability which could be conducive to enhance the performance of smart windows and displays.<sup>2,4</sup> In conventional electrochromic devices, the amorphous WO<sub>3</sub> films have been replaced by crystalline WO<sub>3</sub> films due to their dense structure, high stability and slower dissolution rates in electrolytes. However, their electrochromic performance is affected by slower switching response.<sup>5</sup> To overcome this drawback, large area arrays of nanostructured thin films should be fabricated to improve the electrochromic efficiency. The electrochromic behaviour mainly depends on the morphology, porosity, surface area and surface roughness of the nanostructured electrodes.<sup>6,7</sup>

Till date, nanostructured WO<sub>3</sub> thin films with various surface morphologies, such as 3D nano-urchins, nanoflakes, nanorods, nano-granules, nanowires, mesoporous, nanobricks, etc., have been fabricated by employing several methods, including the sol gel process, spray pyrolysis, thermal evaporation, sputtering, Langmuir-Blodgett, hot-wire chemical vapour deposition, hydrothermal, electrodeposition and layer by layer deposition methods.<sup>8-19</sup> Among the numerous procedures reported for the growth of WO<sub>3</sub> nanostructures, electrodeposition technique is a versatile one because of its advantages, including low growth temperature, facility of

<sup>a</sup> Department of Nanoscience and Technology, Bharathiar University, Coimbatore – 641 046, India. E-mail: dmraj800@yahoo.com

<sup>b</sup> Environmental & Water Technology, Centre of Innovation, Ngee Ann Polytechnic, Singapore 599489, Singapore. E-mail: sureshinphy@yahoo.com

<sup>c</sup> National Institute of Advanced Industrial Science and Technology (AIST), 2266-98 Anagahora, Shimoshidami, Moriyama-ku, Nagoya 463-8560, Japan

<sup>d</sup> Center for Nanofibers and Nanotechnology, Department of Mechanical Engineering, National University of Singapore, Singapore 117576.

† Electronic Supplementary Information (ESI) available

controlling the film thickness, lower cost, high quality, large scale synthesis and unique principle. *Baeck et al*<sup>19</sup> reported the preparation of mesoporous WO<sub>3</sub> thin film by electrodeposition method with enhanced photocatalytic and electrochromic properties. *Ou et al*<sup>20</sup> have fabricated the 3D network like structures by anodization of sputtered WO<sub>3</sub> thin film electrode with enhanced electrochromic efficiency.

To the best of our knowledge, most of the nanostructured thin film electrodes have been fabricated by hydrothermal, solvothermal and physical methods.<sup>12-19</sup> However, there have been no reports on the preparation of vertically aligned 3D Hierarchical WO<sub>3</sub> nanoflake films by the Electrodeposition method. Herein, we demonstrate the design and fabrication of vertically aligned 3D hierarchical WO<sub>3</sub> flower like architectures with porous structure on FTO coated glass substrates via a simple electrodeposition method. Also, we have fabricated the different nanostructured WO<sub>3</sub> thin films such as nanoplatelets with some hierarchical flower like nanospindles with different pH values of the electrolyte. The unique 3D hierarchical flower like nanoarrays are self-assembled by stacking of nanoflakes, which facilitates the easy and fast penetration of ions into the film by shortening the ion diffusion path.<sup>20-22</sup> We have investigated the influence of pH of the electrolyte and deposition time on the nanostructures of WO<sub>3</sub> films. Moreover, the electrochromic performance of all the WO<sub>3</sub> nanostructured thin films as cathodic electrodes have been studied and compared. Compared with nanoplatelets and nanospindles, 3D hierarchical flower like nanoarrays could exhibit outstanding electrochromic performance due to their unique structure.

## 2. Experimental

### 2.1 Synthesis and characterization

All the chemicals used in this work were of analytical reagent grade and purchased from Himedia Co., Ltd., India and used without purification. In a typical synthesis,<sup>19</sup> the precursor solution was prepared by dissolving 1.25g of tungsten (W) powder in 40 ml of hydrogen peroxide (H<sub>2</sub>O<sub>2</sub>) (30%) under constant stirring in a cold bath (0–10 °C) for 24 h. The excess hydrogen peroxide was decomposed by refluxing the solution at 80 °C for 6 h with the addition of glacial acetic acid under stirring after filtering the clear solution. Then the resultant peroxy tungstic acid was diluted to 50 mM with water and isopropanol in 50:50 ratios. The addition of iso-propanol improves the stability of the precursor solution<sup>23</sup> by preventing the precipitation of peroxy complex for an extended period of time (3days). The resulting electrolyte had a pH of 2.21. Different concentrations of oxalic acid were then added to adjust the pH values to 1.51, 0.9 and 0.3. Here the addition of oxalic acid to the precursor is expected to slow down the condensation reaction as well as inhibit the growth of the hydrated tungsten trioxide particles. Also, the addition of the chelating agent into the precursor sol did not lead to the formation of precipitate or gel.<sup>24</sup>

### 2.2 Preparation WO<sub>3</sub> thin films

By using electrolytes with different pH (1.51, 0.9, 0.3) values, three different WO<sub>3</sub> thin films (W1, W2, W3) were deposited under potentiostatic conditions using three electrode electrochemical stations with a platinum wire as the counter electrode, Ag/AgCl as the reference electrode and FTO coated glass with WO<sub>3</sub> seed layer as the working electrode (3×1.5 cm<sup>2</sup>). The electrodeposition was carried out potentiostatically at -0.45 V against the reference electrode at room temperature without stirring for 30 min. The resulting films were rinsed immediately with distilled water and dried in air. The electrodeposited films were then annealed in a muffle furnace at 450 °C for 2 h in air after which structural characterization and electrochromic studies were carried out.

### 2.3 Characterization techniques

The prepared hierarchical WO<sub>3</sub> nanostructured thin films were used as cathodic electrode materials for electrochromic applications and characterized using X-ray diffraction (XRD) pattern obtained using a Panalytical X'Pert Pro with Cu-K<sub>α</sub> radiation (1.5406 Å), X-ray photoelectron spectroscopy (Kratos analytical, ESCA-3400, Shimadzu), FE-SEM (quanta-250), UV-visible spectrophotometer (Jasco V-640), Atomic force microscopy (Veeco di-caliber) and Raman spectroscopy (LABRAM-HR) with laser excitation lines of 514 nm at room temperature. The transmission spectra of WO<sub>3</sub> thin films in the fully colored and fully bleached states were measured in the wavelength range between 300 to 900 nm with a UV-Visible spectrophotometer (Jasco V-640) with FTO coated glass substrate as the reference electrode. The electrochromic properties of the WO<sub>3</sub> thin films were determined from Cyclic Voltammetry (CV), Chrono-amperometry (CA) and Chronocoulometry (CC) techniques using Biologic Science Instruments SP-50 controlled by a personal computer installed with EC-lab software in the three electrode cell configuration with 0.5 M of H<sub>2</sub>SO<sub>4</sub> as the electrolyte, Platinum (Pt) as the counter electrode, Ag/AgCl as the reference electrode and the prepared WO<sub>3</sub> thin film as the working electrode.

## 3. Results and Discussion

### 3.1 Seed layer formation

Prior to the formation of hierarchical WO<sub>3</sub> nanostructures by electrodeposition method, WO<sub>3</sub> seed layer was coated on FTO coated glass substrates by spin coating method. This seed layer is found to play a vital role in the growth mechanism of WO<sub>3</sub> nanostructure. Fig. 1(a) shows the FESEM image of WO<sub>3</sub> seed layer coated on a FTO substrate. Densely piled layers of WO<sub>3</sub> nanocrystals were formed on the FTO substrate after annealing the spin coated seed layer at 500 °C for 2 h. It is evident from the FESEM images that the entire film was covered by WO<sub>3</sub> seed layer which further acts as the nucleation centre for growing WO<sub>3</sub> nanostructures. Fig. 1(b) shows the XRD patterns of the WO<sub>3</sub> seed layer. All the

diffraction peaks can be indexed to monoclinic structure of  $\text{WO}_3$  (JCPDS No. 83-4476), which has strong preferential orientation along (002), (200), (020) planes and will have significant influence on the initial nucleation during the electrodeposition process.

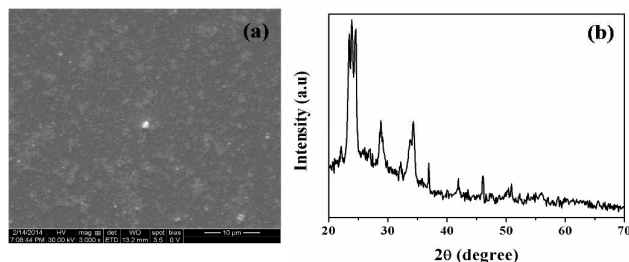


**Fig.1** (a) FESEM images of  $\text{WO}_3$  seed layer on FTO substrate, (b) XRD pattern of  $\text{WO}_3$  seed layer.

### 3.2 Structural analysis

$\text{WO}_3$  nanostructure thin films have been prepared with different pH values of the electrolyte consisting of peroxotungstic acid sol in the presence of an organic acid such as oxalic acid by using electrodeposition technique. The crystalline phase purity and structure of the electrodeposited  $\text{WO}_3$  thin film as functions of the pH value were determined by X-ray diffraction (XRD). The XRD patterns of the  $\text{WO}_3$  thin films W1, W2 and W3 are shown in Fig. 2. All the major diffraction peaks can be indexed to (002), (020), (200), (120), (202), (130), (222), (303), (134), (-234) crystal Planes. All the diffraction peaks are assignable to the monoclinic phase of  $\text{WO}_3$  structure (JCPDS NO 89-4476) and no hydrated  $\text{WO}_3$  is found, indicating the purity of the  $\text{WO}_3$  obtained.

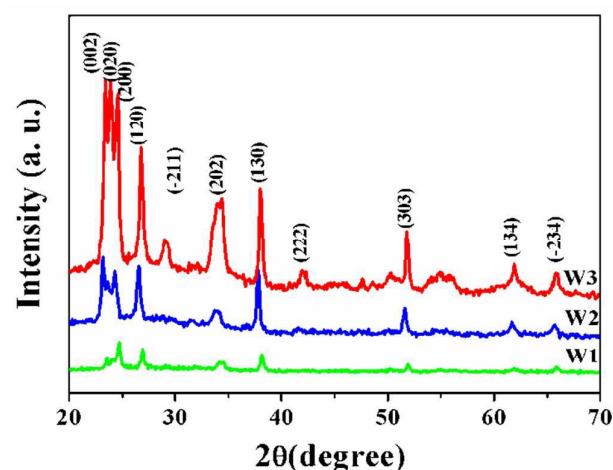


**Fig.2** XRD patterns of electrodeposited  $\text{WO}_3$  thin films: (W1) pH = 1.51, (W2) pH=0.9, (W3) pH = 0.3.

In addition, the intensities of the diffraction peaks are obviously different from each other, revealing different preferred growth directions due to the effect of pH value. The

improved crystallinity will enhance the electrochromic performance of the  $\text{WO}_3$  thin films by reducing the charge transfer resistance during the double injection/ejection of ions and electrons into the  $\text{WO}_3$  film. Thus, the electrodeposited W3 and W2 films exhibit enhanced electrochromic performance compared to the W1 film. These results indicate that addition of organic acid in the electrolyte plays a crucial role in controlling the crystallinity of the  $\text{WO}_3$  thin films

### 3.3 Raman spectroscopy

Raman spectroscopy (Fig. 3 (a-c)) is also used to analyze the phase structure of the  $\text{WO}_3$  thin films. From the three Raman spectra, it is obvious that all the peaks are sharp, thin and well defined due to the crystalline nature of the metal oxide. It can be seen from the Fig. 2 (W3), that the most intense peaks are observed at  $807$  and  $718\text{ cm}^{-1}$ , due to the symmetric and asymmetric vibrations of  $\text{W}^{6+}\text{-O}$  bonds (O-W-O stretching modes), while the bands at  $272\text{ cm}^{-1}$  can be ascribed to the  $\delta$  (W-O-W) bending mode of the bridging oxygen of monoclinic phase.<sup>20,21</sup> This behavior is in good agreement with the Raman shift reported in the literature.<sup>24-26</sup>

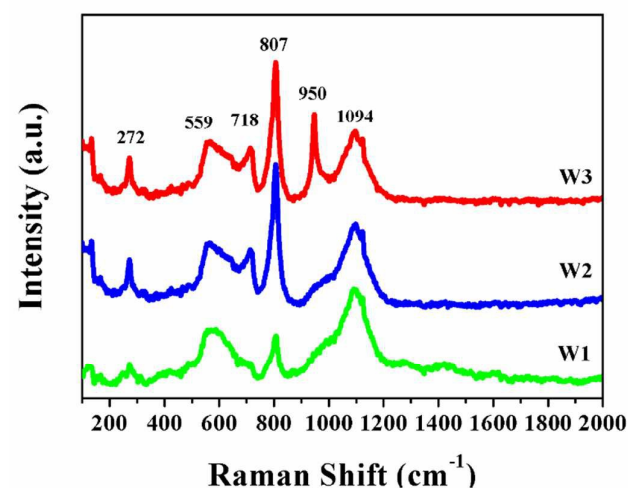


**Fig.3** Raman spectra of  $\text{WO}_3$  thin films: (W1) pH = 1.51, (W2) pH = 0.9, (W3) pH = 0.3.

The relatively sharp bands at  $950\text{ cm}^{-1}$  can be attributed to  $\text{W}^{6+}\text{-O}$  stretching mode of terminal oxygen atoms, which could be possibly located at the surface of the clusters and nano voids in the film and arise due to the development of nanostructures in the film.<sup>31</sup> The bands at  $807$ ,  $717$  and  $272\text{ cm}^{-1}$  arise due to the crystalline nature of  $\text{WO}_3$ . Moreover, films with nanospindles (W1) and nanoplatelets (W3) show results similar to Raman spectra, indicating that all the three samples (W1, W2 and W3) are in the same monoclinic phase of  $\text{WO}_3$  regardless of the different morphologies.

### 3.4 Morphological Analysis

The FESEM images of the as-deposited WO<sub>3</sub> thin films (W1, W2 and W3) are shown in Fig. S1†. The entire film is composed of smooth surface with randomly oriented nanograins which reaffirm the amorphous nature as confirm from XRD pattern of the as-deposited films (Fig. S2†).<sup>32,33</sup> Fig. 4 show the FESEM images of the annealed (450 °C) electrodeposited WO<sub>3</sub> thin films obtained at different pH values by the addition of organic acid. The figure reveals that the annealing process not only manifests in enhancement of orientation and surface grain size but also results in well resolved and highly textured morphology.<sup>34</sup> The observation of triplet peaks along (002), (020) and (200) orientations in XRD pattern (Fig. 1) are evident for the formation of WO<sub>3</sub> films with textured nature. The surface morphology of these films exhibits considerable variations depending on the pH value of the electrolyte. Fig. 4(a-b) shows the FESEM images of the electrodeposited WO<sub>3</sub> thin film when the pH is fixed at 1.51. The entire film has flat and compact small nanospindles like morphology at this stage with thickness ranging from 50 to 90 nm. When the pH is adjusted to 0.9, the WO<sub>3</sub> film is composed of nanoplatelets with increased thickness of about 40-50 nm as in fig. 4 (e-f). Finally, when the pH is decreased to 0.3, the entire film turns out to be composed of homogenously distributed, well aligned hierarchical flower like WO<sub>3</sub> nano arrays with a diameter of 1µm over a large area.

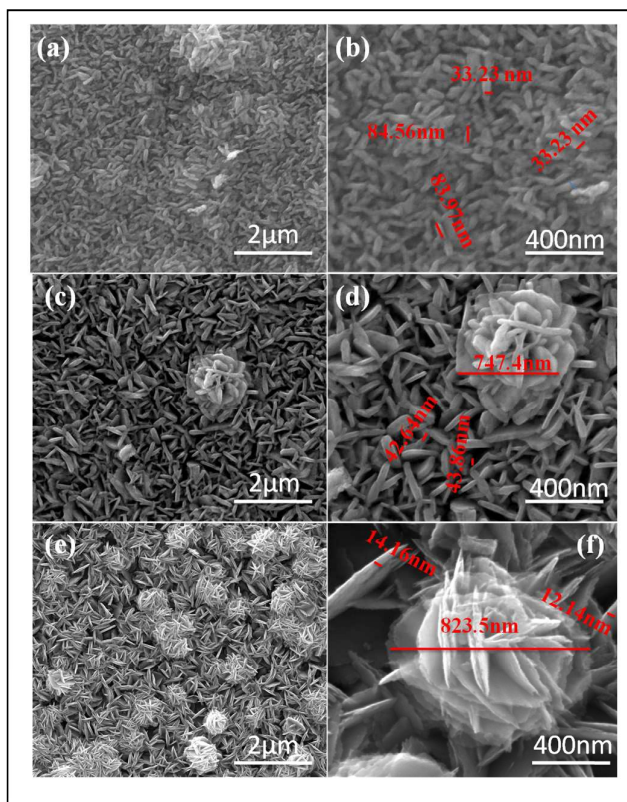


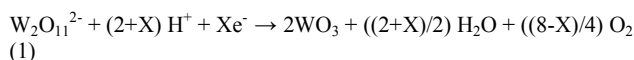
Fig. 4 FESEM images of WO<sub>3</sub> thin films: (a) and (b) pH = 1.51, (c) and (d) pH = 0.9, (e) and (f) pH = 0.3

Further observations from high magnifications divulge that the hierarchical flower like morphology is comprised of self-assembled nanoflakes with thickness ranging from about 10 to 20 nm (Fig. 4(c-d)). Their corresponding cross section images were also shown (Fig. S3†). From these results, we can conclude that decreasing the pH of the electrolyte by means of increasing the concentration of oxalic acid leads to different nanostructures.

The surface topographies of the WO<sub>3</sub> thin films prepared via electrodeposition with different pH values of the electrolyte were characterized by AFM analysis. Parts of the 2D and 3D surface topographies of the WO<sub>3</sub> thin films (W1, W2 and W3) are shown in the Fig. 5 (a-i). Fig. 5(c, f and i) represents the two dimensional histogram which consists of surface height values determined from the respective topographies. In the case of W1 film deposited by using pH of electrolyte at 1.51, the entire substrate surface is populated with spindles like structure with rms surface roughness of 16.22 nm (Fig. 5(a)). Similarly in the case of W2 film, the entire surface consists of nanoplatelets like structure with rms surface roughness of about 21.01 nm (Fig. 5(b)). Meanwhile, the W3 film consists of randomly oriented hierarchical flower like structure over the surface of the film with rms surface roughness of about 47.70 nm. When compared to W1 and W2 films, the W3 film exhibits higher roughness which could be due to formation of larger grains on the surface of the film and increase in the porosity of the films due to the stacking of nanoflakes.<sup>30,35</sup> The presence of voids in the W3 and W2 films into which the charge enters very easily, results in higher optical density which in turn leads to greater electrochromic performance.<sup>36,37</sup> The results obtained in the present study are consistent with those reported earlier; indicating that the electrochromic efficiency and response time are greatly influenced by the porosity, film density and surface roughness of the WO<sub>3</sub> film.<sup>38-40</sup>

#### 3.4.1 Growth Mechanism

The direct cathodic electrodeposition of WO<sub>3</sub> by using Peroxotungstic acid precursor as electrolyte was first reported by *Yamanaka et al.*<sup>25</sup> During the electrodeposition using peroxotungstic acid, the dimer undergoes a reduction leading to the formation of tungsten trioxide and molecular oxygen according to the following equations (1):<sup>23</sup>



#### 3.4.2 Role of Deposition time

In order to elucidate the mechanism of electrodeposited WO<sub>3</sub> thin films, we have deposited the WO<sub>3</sub> film at different deposition times keeping the other parameters constant (electrolyte pH = 0.3, applied potential = -0.45 V). Fig. 6 shows the surface morphologies of the WO<sub>3</sub> films deposited at a constant potential of -0.45 V for different deposition times using FESEM.

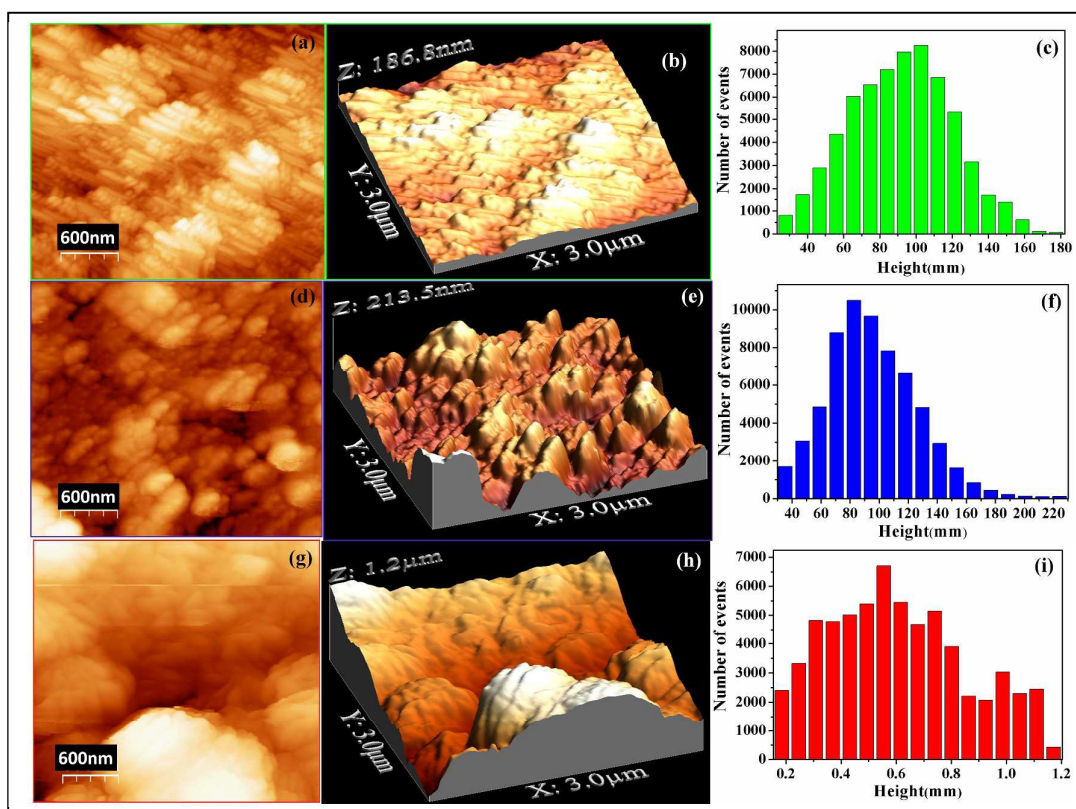


**Fig.5** AFM 2D and 3D images of  $\text{WO}_3$  thin films (a and b) pH = 1.51, (d and f) pH = 0.9, (g and h) pH = 0.3 and (c, f & i) histograms of  $\text{WO}_3$  thin films at different pH (1.51, 0.9, 0.3).

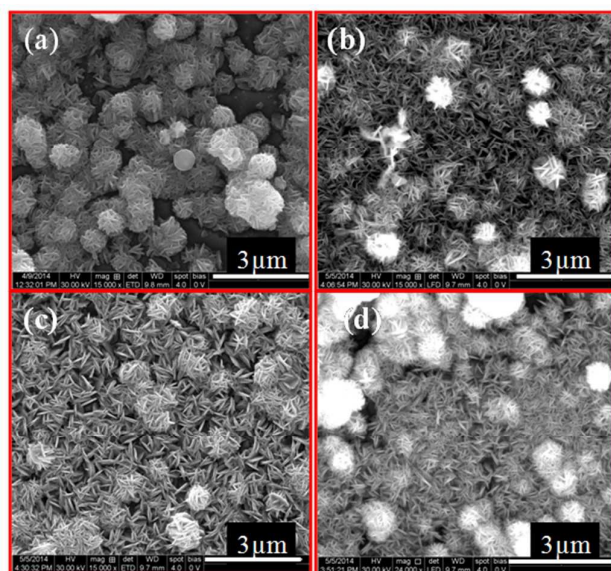


**Fig.6.** FESEM images of the  $\text{WO}_3$  nanostructured thin films (W3) with different deposition times (a) 10min, (b) 20 min, (c) 30 min, (d) 45min.

It is observed that, in the initial stage, the  $\text{WO}_3$  nano particles on FTO act as seeds for the nucleation, paving the way for faster growth of  $\text{WO}_3$  nuclei along these directions ((002), (020) and (200) planes) due to the exact lattice match forming small nanoflakes during the first 10min (Fig.6 (a)). When the deposition time is increased to 20 min, the small nanoflakes progressively grow to form longer nanoflakes like structure (Fig.6 (b)). After the monolayer of nanoflakes was formed, on further increasing the deposition time to 30 min, the nanoflakes tend to coalesce to form hierarchical nanoflakes like structures (Fig.6 (c)). On further increasing the deposition time, the hierarchical nanoflakes like structures grow continuously by stacking of the nanoflakes (Fig.6 (c-d)). From these results it is obvious that initially isolated nuclei were formed on seed substrate and then the nuclei progressively grew to form larger particles and on increasing the deposition time the particles tended to coalesce to form a linked network and then finally formed a uniform layer by continuous deposition. Our results are in consistent with the growth mechanism of electrodeposited tungsten oxide films described by *Shen et al.*<sup>41</sup> Analogously, the same mechanisms have been observed for the other pH values of the electrolyte regardless of the different morphologies (**Fig.S4†**, **Fig.S5†**).

### 3.4.3 Role of the pH of the electrolyte

Fig.7 illustrates the schematic representation of formation mechanism and morphological evolution of the  $\text{WO}_3$  thin films depending on the different pH values (0.3 – 1.51) obtained by adding organic acid. Previous reports show that oxalic acid has a role as a stabilizing agent, in which the small ligand molecules  $\text{H}_2\text{C}_2\text{O}_4$  could coordinate with  $\text{W}^{6+}$  to stabilize the tungstic acid sol during the formation of tungsten oxide thin films.<sup>42,43</sup> Reports also show that oxalic acid acts as a surfactant which could prevent the tungstic acid micro particles from coagulation so as to prepare nanostructured  $\text{WO}_3$  films.<sup>24</sup>

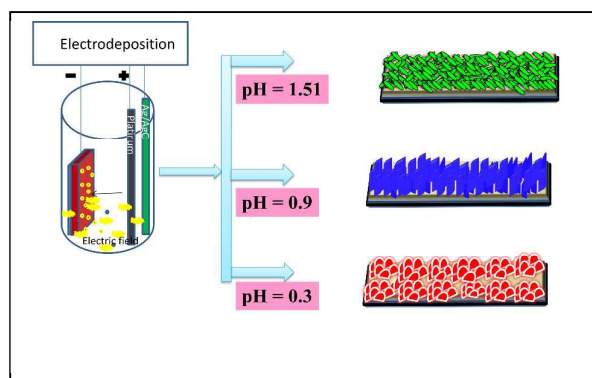


**Fig.7.** Schematic illustrations of growth mechanism of the  $\text{WO}_3$  nanostructured thin films.

The effect of carboxylic acid in the synthesis of  $\text{WO}_3$  by electrodeposition was first observed by *Kwong et al.*<sup>44</sup> They observed that these hydronium ions cause the deflocculation and the conjugate base separated the ion complex that leads to control the distribution density of the  $\text{WO}_3$  nuclei, their proximity, corresponding diffusion coefficient and tendency to form grains during annealing and also suppresses the solute clustering immediately prior to electrodeposition.<sup>40</sup> In the present work, the increase in concentration of the oxalic acid decreases the pH of the electrolyte, resulting in increase of the thickness of the film and enhancing the crystallinity, preventing the agglomeration and also leading to a different morphology. This clearly indicates its active role as a stabilizer and pH inducer like an organic acid.<sup>45</sup> These results are in agreement with results obtained by *Kwong et al.*, who reported that increasing the concentration of oxalic acid in the electrolyte not only prevents the degree of aggregation but also increases the thickness of the electrodeposited  $\text{WO}_3$  thin film.<sup>44,45</sup>

At a low concentration of oxalic acid (0.01 M), the pH of the electrolyte is 1.51. When an organic acid like oxalic acid is dissolved in PTA solution, it will dissociate into hydronium ions and conjugate base. These hydronium ions form a net positive charge around the PTA surface through hydrogen bonding. During the electrodeposition, PTA ions are driven by the electric field towards the working electrode and form a  $\text{WO}_3$  nanostructure through reduction at the surface of the working electrode. The excess hydronium ions and oxalate were

removed on annealing at 450 °C, which is confirmed by FTIR spectra. At pH 1.51, small nanoflakes(spindles) like morphology was obtained as seen from the FESEM images (Fig. 4(a-b)) discussed earlier, where the thickness of the nanospindles was in the range from 50 to 90 nm. On increasing the concentration of oxalic acid to 0.05 M, a greater number of hydronium ions are available thereby decreasing the pH of the electrolyte which leads to well aligned nanoplates like structure by stacking of nanoplates formed with thickness ranging from 40 to 50 nm as shown in Fig. 4(b). On further increasing the concentration of oxalic acid, the availability of hydronium ions is increased further, which leads to decrease in pH to 0.3 which in turn leads to well defined hierarchical flower like array of assembled  $\text{WO}_3$  nanoflakes with thickness in the range from 10 to 20 nm. Larger spacing and numerous pores are formed between adjacent nanoflakes which pave the way for easy ion diffusion from the electrolyte into the  $\text{WO}_3$  film. Pores are observed between the stacked nanoflakes surfaces which may be due to rapid delamination, which in turn occurs due to the separation effect of the conjugate bases of oxalic acid and also due to the release of water molecules during the annealing process that convert  $\text{WO}_3 \cdot n\text{H}_2\text{O}$  to  $\text{WO}_3$ .<sup>44</sup> The entire film is devoid of cracks due to the addition of organic acid in peroxotungstic acid.<sup>46</sup> In the absence of the oxalic acid, the electrodeposited  $\text{WO}_3$  films consist of randomly oriented nanoplates like morphology with some cracks (**Fig.S6†**). From these results, it can be concluded that, oxalic acid plays a vital role as a stabilizer, pH inducer and directing agent during the growth of the nuclei and crystal growth of different nano architectures occurred via the electrodeposition process.

### 3.5 UV-Vis spectra and bandgap

Fig.8 compares the optical properties of the  $\text{WO}_3$  films deposited with different pH values of the electrolyte by the electrodeposition method. It is revealed from Fig. 8(a) that, the optical transmittance for the hierarchical flower like nano array film (W3) is under 68% in the visible-light region, which is much lower than that of the plate like film (W2) and nanospindles like film (W1) (80-84%). The main reason for the low transmittance value of W3 is owing to the high rms surface roughness value and porosity in the stacking of the nanoflakes. With reference to the lower reflectance spectra as shown in Fig.8(b), absorption spectra of the porous  $\text{WO}_3$  film (W3) have been assessed according to the relation,  $A = 100 - R - T$  (Fig. 8(c)), which exhibits higher absorption ability than the W2 and W1 films owing to the increased light absorption paths among the hierarchical flower like arrays by the stacking of nanoflakes.<sup>47</sup> The optical bandgap values for the three samples are found to be 2.82, 2.51 and 2.47 eV for W1, W2 and W3 respectively which are shown in **Fig. S7†**. The variation in bandgap induced by the degree of crystallinity<sup>48</sup> as well as the orientation<sup>49</sup> of the nanostructure on the FTO substrate.<sup>50</sup> These results are in good agreement with an earlier report<sup>48</sup> according to which the degree of crystallinity of  $\text{WO}_3$  could affect its band gap width.

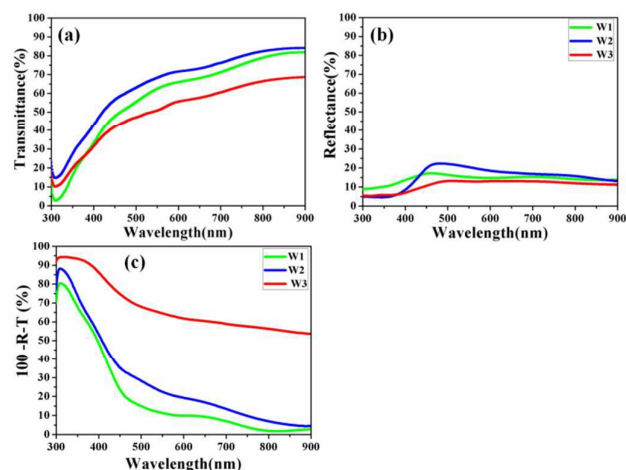


**Fig. 8** UV-Visible spectra of nanospindles(W1) , nanoplatelets (W2) and Hierarchical flower like (W3) thin film (a) Transmittance spectra, (b) Reflectance spectra ,(c) absorption (100-R-T) spectra.

### 3.5.1 Porosity of Three-Dimensional WO<sub>3</sub> nano Structure

A nanoporous WO<sub>3</sub> film for the electrochromic device is vital to enhance the permeation of the electrolyte to the entire structure. For electrochromic application, it is highly enviable that the WO<sub>3</sub> film has a rough and porous surface, so that it is more conducive to provide the short diffusion pathway for the counter ions as well as large active surface, thereby reducing the response time and enhancing the optical modulation. The porosity of the films not only enhances the surface area and ion-insertion kinetics, but also reduces the overall material cost, leading to an inexpensive, large-area EC material. Lee et al.<sup>51</sup> reported that the porous structure of the sputtered WO<sub>3</sub> thin films deposited at large target substrate distance show excellent electrochromic performance when compared to the films sputtered at shorter target-substrate distance. Xia et al.<sup>52</sup> reported that NiO thin films showed good reaction kinetics with fast switching time due to its highly porous structure. In order to understand the porous structure of electrodeposited WO<sub>3</sub> films, we have to determine the porosity of the film. By substituting the values of refractive index of each film in the equation (5) (EIS S9†), the porosity values of the W1, W2 and W3 were calculated as shown in Table 1(Fig. S13†). The hierarchical flower like nanoflakes array show higher porosity (about 50.28%) than the nanoplatelets (31.01%) and nanospindles (18.28%) like morphology. As shown in Fig. S8†, the low refractive indices of W3 and W2 films are due to the high porosity.<sup>53,54</sup> The high porosity of the W3 and W2 films

will make their electrochromic performance better than that of the W1 film by minimizing the time of optical modulation and enhancing the intercalation and de-intercalation of protons during the electrochromic process.

### 3.6 X-ray photoelectron spectroscopy (XPS)

By analyzing the chemical binding states of W, the stoichiometry, surface composition, and chemical surface states of the electrodeposited WO<sub>3</sub> thin films were evaluated by X-ray photoelectron spectroscopy (XPS). Typical survey spectra of the electrodeposited WO<sub>3</sub> thin films are shown in Fig.S10†(c), (f) and (i).

The XPS spectra show only tungsten, oxygen and also a trace amount of carbon, owing to the surface contamination. The spectra of W4f core level and O1s are presented in the Fig. S10(a,b)† for the tungsten oxide nanospindles (W1). The W4f core level of W1 film was dominated by spin orbit doublet at binding energy of 35.0 and 37.1 eV for W4f<sub>7/2</sub> and W4f<sub>5/2</sub> respectively with the spin-orbit separation (W4f<sub>7/2</sub> – W4f<sub>5/2</sub>) of about 2.1 eV. The energy position of this doublet corresponds to the 6+ valence state of W.<sup>55</sup> The O1s spectrum shows two peaks located at 530.2 and 532.4 eV in Fig. S10(b)†. The former peak was assigned to the W=O bonding modes in stoichiometric WO<sub>3</sub>.<sup>56</sup> The latter small peak was assigned to the oxygen from atmospheric water molecules bound with WO<sub>3</sub> film structure or adsorbed on the surface of the film.<sup>57,58</sup> Similarly, the W4f spectrum of the WO<sub>3</sub> nanoplatelets film (W2) (Fig. S10(d)†) can also be dominated by spin orbit doublet at similar binding energies of about 35.0 and 37.1 eV. The O1s spectrum of the WO<sub>3</sub> nanoplatelets film (W2) shows a peak located at 530.2 eV (Fig. S10(e)†), which was also assigned to the W=O bonding modes in the stoichiometric WO<sub>3</sub>. The intensity of the O1s peak(Fig. S10(e)†) gets increased as compared to that of the nanospindles WO<sub>3</sub> film (W1), suggesting that decreasing the pH of the electrolyte by increasing the oxalic acid concentration, causes subsequent improvement in the stoichiometry of the WO<sub>3</sub> nanoplatelets film (W2). W4f and O1s spectra of the WO<sub>3</sub> hierarchical flower like nanostructured film (W3) are shown in Fig. S10(g)† and Fig. S10(h)†. Spectra of the W4f peaks are dominated by the spin orbit doublet with similar binding energies of about 35.0 and 37.1 eV. The intensity of the O1s peak is increased as compared to that of the W1 and W2 films, suggesting that the stoichiometry of the WO<sub>3</sub> hierarchical flower like nanostructured film (W3) is enhanced on decreasing the pH of the electrolyte by increasing the concentration of oxalic acid.

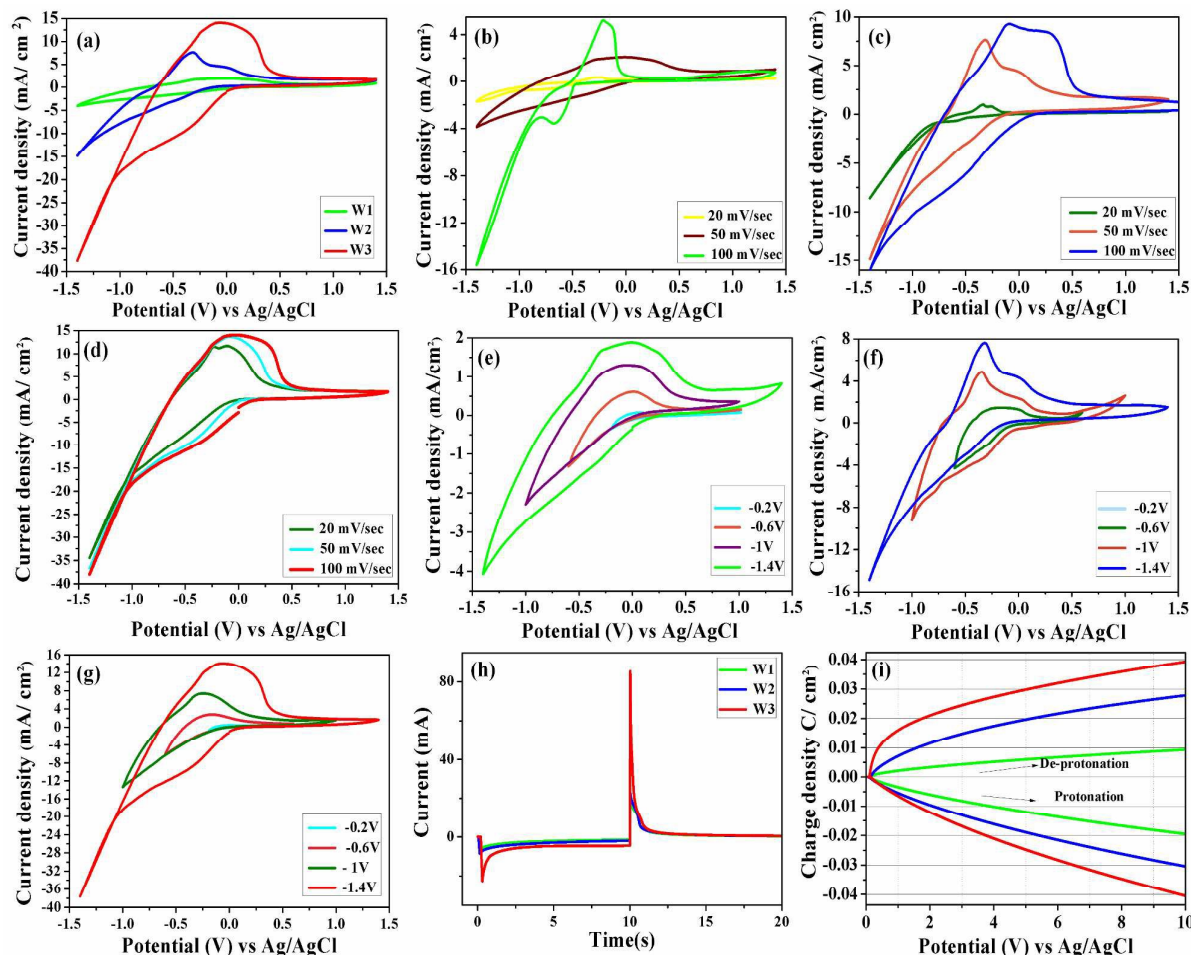


**Fig.10** (a) CVs of the  $\text{WO}_3$  thin films at a scan rate of  $50 \text{ mV s}^{-1}$ . (b) CVs of W1 (nanospindles) film at different scan rate. (c) CVs of W2 (nanoplatelets) film at different scan rate. (d) CVs of W3 (3D hierarchical flower) film at different scan rate. (e) CVs of W1 film at different applied voltage. (f) CVs of W2 film at different applied voltage. (g) CVs of W3 film at different applied voltage. (h) Chronoamperometric (CA) response of the  $\text{WO}_3$  thin films. (i) Plotting indicating differences in Chronocoulometry measurement for the W1, W2 and W3 electrodes.

These observations reveal that all the three nanostructured  $\text{WO}_3$  thin films were fully oxidized and correspond to stoichiometric  $\text{WO}_3$  which is confirmed by XRD patterns.

### 3.8 Electrochemical Studies

In order to evaluate the effect of the morphology of electrodeposited  $\text{WO}_3$  thin films on their electrochromic properties, typical cyclic voltammogram (CV) technique is employed to examine the cathodic and anodic behaviour of electrochromic  $\text{WO}_3$  thin films. These CV are normalized with respect to the constant geometrical effective area  $4.5 \text{ cm}^2$  (dimension  $3 \text{ cm} \times 1.5 \text{ cm}$ ) of the electrodes. Fig.10 (a) compares the CV curves of nanospindles (W1), nanoplatelets (W2) and hierarchical flower (W3)  $\text{WO}_3$  thin film electrodes obtained at a scan rate of  $50 \text{ mVs}^{-1}$  using  $0.5 \text{ M H}_2\text{SO}_4$  electrolyte and a potential window of  $-1.4 \text{ V}$  to  $+1.4 \text{ V}$ . During

the cathodic scan by applying the potential of about  $-1.4 \text{ V}$ , intercalation of electrons and  $\text{H}^+$  ions into the electrode leads to reduction of  $\text{W}^{6+}$  ionic state to  $\text{W}^{5+}$  state resulting in the formation of a blue colored tungsten bronze ( $\text{H}_x\text{WO}_3$ ).<sup>59</sup> On the contrary, during the anodic scan, the tungsten bronze ( $\text{H}_x\text{WO}_3$ ) oxidized into its original  $\text{WO}_3$  form due to oxidation of  $\text{W}^{5+}$  to  $\text{W}^{6+}$  as a consequence of deintercalation of  $\text{H}^+$  ions and electrons from the film. The mechanism underlying intercalation/deintercalation of ions and electrons in an electrochromic  $\text{WO}_3$  film can be described by the equation:<sup>60</sup>



From the CV plots, the calculated diffusion coefficients of W1, W2 and W3 were  $4.9068 \times 10^{-7}$ ,  $6.792 \times 10^{-7}$ ,  $1.847 \times 10^{-6} \text{ cm}^2 \text{ s}^{-1}$  (intercalation) and  $2.931 \times 10^{-7}$ ,  $3.7892 \times 10^{-7}$  and  $7.196 \times 10^{-7} \text{ cm}^2 \text{ s}^{-1}$  (deintercalation) respectively (**EIS S10†**).

## Journal Name

## ARTICLE

From the CV plot, it is observed that W3 electrode and W2 electrode show significantly larger current densities compared to that of W1 electrode which reflects the fact that hierarchical flower like nanoarray and nanoplatelets provide an easy way for diffusion and charge transfer process of ions in the WO<sub>3</sub> film. Moreover, while comparing the W2 and W3 films, the cathodic and anodic peak currents of W3 film electrode are four times higher than that of W2 film electrode. The enhanced electrochromic behaviour is mainly attributed to its unique 3D hierarchical flower like architectures. The 3D hierarchical flower like architectures were self assembled by stacking of numerous ultrathin porous nanoflakes providing more active sites, which could be conducive to enhance electrolyte ions transportation on the surface of the active materials and throughout the bulk.<sup>61,62</sup> Furthermore, the porosity in the nanoflakes and nanoplatelets will play a vital role in shortening ion diffusion length between the external electrolyte and interior surfaces by serving as "ion reservoir".<sup>21,22</sup> By using the equation (5), the porosity values of WO<sub>3</sub> nanostructured thin films were found to be 18.28% for nanospindles, 31.01% for nanoplatelets and 50.28% for hierarchical flower like architectures. From these results, it is revealed that the W3 film electrode exhibits higher porosity than the W2 and W1 film electrodes, which attributes to the enhanced electrochromic behaviour. The onset potential of the cathodic peak current shifted to more positive potentials for both the electrodes, owing to the reduced interfacial charge transfer resistance.<sup>20</sup>

Fig. 10(b-d) shows the CV curves for the W1, W2 and W3 electrodes at different scan rates from 20 to 100 mV/ s. From Fig. 10(d), both the oxidation and reduction peak currents increases upon increasing the scan rate with slight shift in the oxidation peak current, which could be ascribed to the fact that the amount of H<sup>+</sup> ions and electrons incorporated into the film increases at the larger scan rate. On the other hand, W1 and W2 film electrodes exhibit larger shift in the oxidation peak current as shown in the Fig. 10(b-c). From these results, it is revealed that the W3 film electrode exhibits faster insertion kinetics, when compared to the W2 and W1 film electrodes. Moreover, the CV curves of WO<sub>3</sub> film electrode at a scan rate of 50 mVs<sup>-1</sup> between different applied voltages range from -0.2, -0.6, -1 and -1.4 V respectively are compared as shown in Fig.10 (e-g). It was observed that when the potential window is stepped from +1.4 to -0.2 V at a constant scan rate of 50 mV/sec the W3 film shows a higher cathodic current density when compared to the W2 and W1 electrodes which is attributed to the hierarchical flower like nanoarray.

The switching kinetics is the important criterion to determine the practical applications of electrochromic films. The time required for a 90% change in optical transmittance between colored and bleached states is termed as switching kinetics. The coloration and bleaching response times of W1, W2 and W3 electrodes are estimated from current time transients.<sup>63</sup> Typical chronoamperometry (CA) traces of the WO<sub>3</sub> film electrodes were recorded by applying alternative voltage of ±1 V for 10 s as shown in the Fig. 10(h). The WO<sub>3</sub> electrode gets darkened during negative sweep (-1.0 V), owing to the intercalation of protons and electrons into the film and gets bleached due to the deintercalation during positive sweep voltage (1.0 V). The estimated switching time for coloration state (t<sub>c</sub>) and bleaching state (t<sub>b</sub>) of W1, W2 and W3 film electrodes from the current transient plot are listed in the Table 1 (Fig. S13†). The W3 film electrode exhibits faster coloration and bleaching times of 5.05 s and 3.82 s respectively, which are faster than those of W2 and W1 electrodes. The faster switching kinetics of the W3 film electrode is ascribed to enhanced crystallinity and higher surface roughness (46 nm), which are conducive for enhancement of intercalation/deintercalation behavior of H<sup>+</sup> ions by facilitating the contact between external ions and the oxide surface. This is confirmed from the CV plot in which the cathodic current shifted towards the positive potential due to availability of more coarse surface leads for quick H<sup>+</sup> ion movement and greater electronic conductivity.<sup>64,65</sup> Furthermore, the freestanding hierarchical flower array with open spaces between the individual nanoflakes allows the easy diffusion of ions.<sup>66</sup>

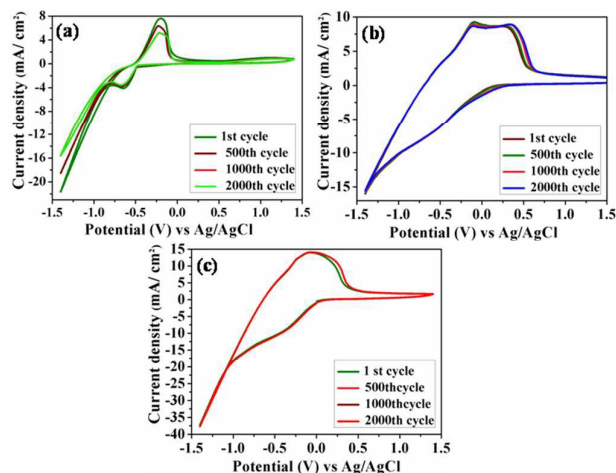
Chronocoulometry measurements of WO<sub>3</sub> electrode were carried out at voltage sweep ranging from -1.0 to +1.0 V with steps of 10 s in order to estimate H<sup>+</sup> ion intercalation and deintercalation. Fig. 10(i) represents the plot of charge vs. time transient. During the diffusion process by applying the positive voltage, the charges are intercalated into the film, resulting in coloration due to the reduction of W<sup>6+</sup> to W<sup>5+</sup> states.<sup>67</sup> In the reverse conditions, during negative scan, the films turned colorless (bleached) by removal of intercalated charge from the film due to oxidation of W<sup>5+</sup> to W<sup>6+</sup> states. The reversibility of the films is calculated depending on the ratio of the deintercalated charge (Q<sub>di</sub>) to the intercalated charge (Q<sub>i</sub>) for coloration/bleaching after 10 seconds using the following equations (9):<sup>20</sup>

$$\text{Reversibility} = \frac{Q_{di}}{Q_i} \quad (9)$$

The estimated percentage of electrochromic reversibility for all the WO<sub>3</sub> film electrodes has been listed in Table 1 (Fig. S13†). The W3 electrode shows excellent reversibility of about 94.11%, since it offers a well-defined crystalline structure, high porosity (50.28%) and hierarchical flower-like surface morphology.

### 3.9 Stability Study

In order to investigate the electrochemical stability of all the WO<sub>3</sub> film electrodes, a typical cyclic voltammogram (CV) is carried out at a potential of  $\pm 1.4$  V at a scan rate of 50 mV s<sup>-1</sup> using 0.5 M H<sub>2</sub>SO<sub>4</sub> as the working electrolyte.



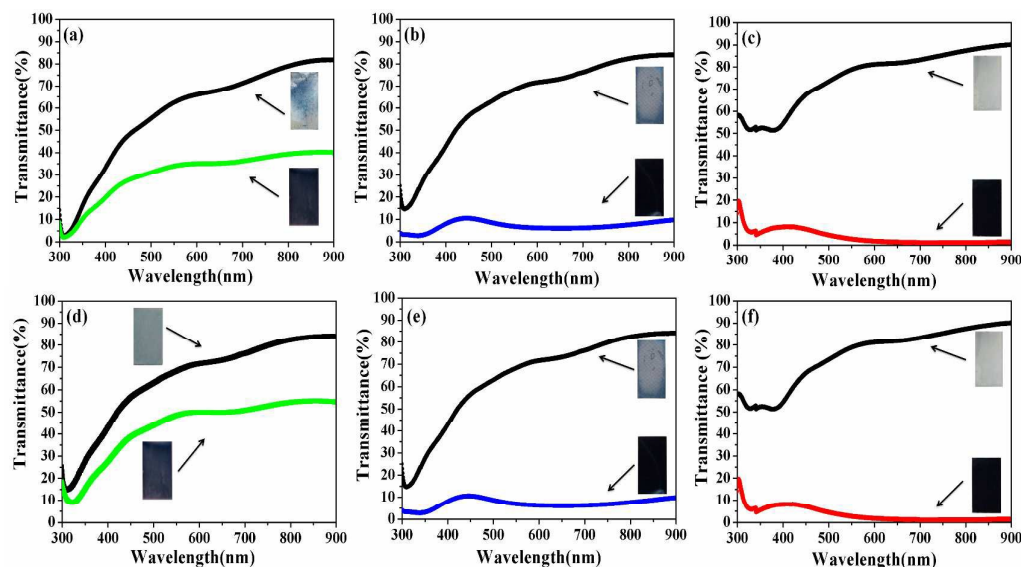
**Fig. 11** CVs cyclic stabilities of the WO<sub>3</sub> thin films (a) W1, (b) W2 and (c) W3.

Fig. 11(a-c) represents the CV curves at 1st, 500th, 1000th and 2000th cycles at room temperature for W1, W2 and W3 electrodes. From Fig. 11(c), it can be seen that the W3 electrode shows excellent stability with a stable current response without significant change in the shape of the CV curve, while the W2 electrode shows higher stability with a slight reduction in the current densities. The difference could be attributed to different surface morphology and porous WO<sub>3</sub> architectures which can provide structural flexibility for volume change during the repeated insertion/extraction of H<sup>+</sup> ions.<sup>62</sup> Contrastingly, W1 film shows a slow and significant decrease in the current density from the first cycle to the 2000th cycle due to its low crystallinity and very low porosity which may control the H<sup>+</sup> ion intercalation/deintercalation into the surface.<sup>65</sup>

### 3.10 Coloration properties of WO<sub>3</sub> electrodes

Another important criterion to develop the EC system is the optical transparency of the electrochromic films. Coloration and bleaching of the WO<sub>3</sub> thin film were carried out by applying the potential sweep of  $\pm 1.2$  V for a fixed time.

The UV-visible transmittance spectroscopy was performed in the 300–900 nm wavelength range at room temperature for the WO<sub>3</sub> thin film electrodes in its colored and bleached states after 1<sup>st</sup> and 2000<sup>th</sup> cycles (Fig. 12). It is seen in this figure that the optical transparency decreases when the WO<sub>3</sub> film is cathodically polarized and subsequently increases due to bleaching of the electrodes.<sup>68</sup> The changes in optical modulation for all the WO<sub>3</sub> film electrodes are listed in Table 1 (Fig. S13†). From Fig. 12(a) the transmittance values for the colored and bleached states of W3 film electrode at the visible wavelength of 550 nm were found as  $T_c = 2.52\%$  and  $T_b = 79.90\%$  respectively. It can be seen from Fig. 12(d-f) that the optical transmittance spectra of the electrodes remain the same after 2000 cycles with slight variation in the case of W1 electrode. As previously conferred, cyclic stability studies illustrate that W3 and W2 electrodes have excellent stability even after the 500<sup>th</sup> cycle and up to 2000 cycles. Therefore, it is obvious to believe that optical transmittance spectra of the W3 and W2 electrodes also remain stable till 2000<sup>th</sup> cycle. The coloration efficiency of W1, W2 and W3 thin film electrodes calculated from equation (8) (ESI S12†) were found to be 59.34 cm<sup>2</sup> C<sup>-1</sup>, 142.83 cm<sup>2</sup> C<sup>-1</sup> and 172.08 cm<sup>2</sup> C<sup>-1</sup> respectively. The W3 film electrode exhibits much higher CE efficiency compared to the W2 and W1 films due to the unique 3D hierarchical flower-like arrays. Furthermore, the estimated CE value of W3 film electrode is also much higher than those of the different morphologies reported: nanowire array film (102.8 cm<sup>2</sup> C<sup>-1</sup>),<sup>69</sup> nanocuboids (60.17 cm<sup>2</sup> C<sup>-1</sup>),<sup>70</sup> nanofibres (129.2 cm<sup>2</sup> C<sup>-1</sup>),<sup>71</sup> nanoplates (38.2 cm<sup>2</sup> C<sup>-1</sup>),<sup>72</sup> platelet-like hydrated WO<sub>3</sub> film (112.7 cm<sup>2</sup> C<sup>-1</sup>),<sup>73</sup> nanoporous film (141.5 cm<sup>2</sup> C<sup>-1</sup>),<sup>20</sup> hierarchical nanotrees (102.85 cm<sup>2</sup> C<sup>-1</sup>),<sup>13</sup> nanospheroids (42.5 cm<sup>2</sup> C<sup>-1</sup>),<sup>74</sup> nanopores (58 cm<sup>2</sup> C<sup>-1</sup>)<sup>75</sup> and nanorods (42.5 cm<sup>2</sup> C<sup>-1</sup>).<sup>76</sup> According to these results, we can conclude that superior improvement in CE value of W3 film could be mainly ascribed to an increased porosity due to the stacking of nanoflakes and orientation of flower-like assemblies. The increased porosity would have paved the way for the larger active surface area for charge transfer reaction compared to the W2 and W1 films.



**Fig.12** Optical transmittance spectra of the colored and bleached states of WO<sub>3</sub> thin film electrodes: (a-c) W1, W2 and W3 after 1<sup>st</sup> cycle, (d-f) W1, W2 and W3 after 2000 cycle.

#### 4. Conclusion

vertically aligned 3D hierarchical flower (W3) like WO<sub>3</sub> nanostructured thin films have been synthesized by using electrodeposition method. By tuning the pH of the electrolyte, variety of WO<sub>3</sub> nanostructures such as nanospindles, nanoplatelets, heirarchical flower nanoarray were obtained. Oxalic acid in the electrolyte plays an important role in determining the surface morphology. The hierarchical flower like nanoarrays(W3) exhibit superior electrochromic performance compared to that of the nanoplatelets and nanospindles like morphology. The hierarchical flower WO<sub>3</sub> like nanoarrays is formed by stacking of atomically thin nanoflakes, leading to higher surface roughness and porosity which control and facilitate ions insertion kinetics, leading to a superior electrochromic performance. The nanostructured WO<sub>3</sub> thin film electrode(W3), electrodeposited at pH = 0.3, exhibits an excellent electrochromic behaviour with larger optical contrast (79.90% at 550 nm), faster switching response time ( $t_b = 3.82$  s and  $t_c = 5.05$  s), and superior coloration efficiency ( $172.08 \text{ cm}^2 \text{ C}^{-1}$ ) and stability over 2000 cycles. Our results suggest that 3D hierarchical flower like WO<sub>3</sub> nanoarray electrode synthesized by electrodeposition has great impact on the large scale production and makes the material a promising candidate for fabrication of EC devices.

#### Acknowledgement

One of the authors S. P gratefully acknowledges the DST-PURSE, Government of India for the FESEM facility.

#### References

- P. Suresh Kumar, J. Sundaramurthy, S. Sundarrajan, V. Jagadeesh Babu, Gurdev Singh, S. I. Allakhverdiev and S. Ramakrishna, *Energy Environ. Sci.*, 2014, **7**, 3192.
- C. G. Granqvist, *Sol. Energy Mater. Sol. Cells*, 2000, **60**, 201.
- D. Ma, H. Wang, Q. Zhang and Y. Li, *J. Mater. Chem.*, 2012, **22**, 16633.
- J. Zhang, J. P. Tu, D. Zhang, Y. Q. Qiao, X. H. Xia, X. L. Wang and C. D. Gu, *J. Mater. Chem.*, 2011, **21**, 17316.
- S. H. Lee, R. Deshpande, P. A. Parilla, K. M. Jones, B. To, A. H. Mahan and A. C. Dillon, *Adv. Mater.* 2006, **18**, 763.
- C. G. Granqvist, E. Avendano and A. Azens, *Thin Solid Films*, 2003, **442**, 201.
- J. Zhang, J. P. Tu, G. F. Cai, G. H. Du, X. L. Wang and P. C. Liu, *Electrochim. Acta*, 2013, **99**, 1.
- Z. Jiao, J. Wang, L. Ke, X. Liu, H. V. Demir, M. F. Yang and X. W. Sun, *Electrochim. Acta*, 2012, **63**, 153.
- Z. J. Gu, T. Y. Zhai, B. F. Gao, X. H. Sheng, Y. B. Wang, H. B. Fu, Y. Ma and J. N. Yao, *J. Phys. Chem. B*, 2006, **110**, 23829.
- G. Xi, J. Ye, Q. Ma, N. Su, H. Bai and C. Wang, *J. Am. Chem. Soc.* 2012, **134**, 6508.
- F. Kim, S. Kwan, J. Akana and P. D. Yang, *J. Am. Chem. Soc.* 2001, **123**, 4360.
- Z. S. Houweling, J. W. Geus, and R. E. I. Schropp, *Chem. Vap. Deposition*, 2010, **16**, 179.
- J. Zhang, X. L. Wang, X. H. Xia, C. D. Gu and J. P. Tu, *Sol. Energy Mater. Sol. Cells*, 2011, **95**, 2107.
- C. Santato, M. Odziemkowski, M. Ulmann and J. Augustynski, *J. Am. Chem. Soc.* 2001, **123**, 10639.
- M. Regragui, M. Addou, A. Outzourhit, Elb. El Idrissi, A. Kachouane and A. Bougrine, *Sol. Energy Mater. Sol. Cells*, 2003, **77**, 341.
- X. G. Wang, Y. S. Jang, N. H. Yang, Y.M. Wang, L. Yuan and S. J. Pang, *Sol. Energy Mater. Sol. Cells*, 2000, **63**, 197.

## Journal Name

## ARTICLE

- 17 Y. Baek and K. Yong, *J. Phys. Chem. C*, 2007, **111**, 1213.
- 18 S. J. Choi, S. J. Kim, W. T. Koo, H. J. Cho, and I.D. Kim, *Chem. Commun.*, 2015, **51**, 2609.
- 19 S. H. Baeck, K. S. Choi, T. F. Jaramillo, G. D. Stucky and E. W. McFarland, *Adv. Mater.* 2003, **15**, 1269.
- 20 J. Ou, S. Balendhran, M. R. Field, D. G. McCulloch, A. S. Zoofakar, R. A. Rani, S. Zhuiykov, A. P. O'Mullaneb and K. K. Zadeh, *Nanoscale*, 2012, **4**, 5980.
- 21 K. Xu, R. Zou, W. Li, Y. Xue, G. Song, Q. Liu, X. Liu and J. Hu, *J. Mater. Chem. A*, 2013, **1**, 9107.
- 22 X. Lang, A. Hirata, T. Fujita and M. Chen, *Nature Nanotechnology*, 2011, **6**, 232.
- 23 E. A. Meulenkamp, *J. Electrochem. Soc.*, 1997, **144**, 1644.
- 24 M. U. Sun, X. U. Ning, Y. W. Cao, J. N. Yao and E. G. Wang, *J. Mater. Sci. Lett.* 2000, **19**, 1407.
- 25 K. Yamanaka, H. Oakamoto, H. Kidou and T. Kudo, *Jpn. J. Appl. Phys.*, 1986, **5**, 1420.
- 26 R. F. G. Sanchez, T. Ahmido, D. Casimir, S. Baliga and P. Misra, *J. Phys. Chem. A*, 2013, **117**, 13825.
- 27 M. F. Daniel, B. Desbat, J. C. Lassegues, B. Gerand and M. Figlarz, *J. Solid State Chem.*, 1987, **67**, 235.
- 28 N. Wang, D. Wang, M. Li, J. Shi and C. Li, *Nanoscale*, 2014, **6**, 2061.
- 29 M. Breedon, P. Spizzirri, M. Taylor, J. du Plessis, D. McCulloch, J. Zhu, L. Yu, Z. Hu, C. Rix, W. Wlodarski and K. Kalantar-zadeh, *Cryst. Growth Des.*, 2010, **10**, 430.
- 30 N. Kakati, S. H. Jee, S. H. Kim, J. Y. Oh and Y. S. Yoon, *Thin Solid Films* 2010, **519**, 494.
- 31 N. Santo, M. Filipescu, P. M. Ossi and M. Dinescu, *Appl. Phys.*, A, 2010, **101**, 325.
- 32 G. R. Jafari, A. A. Saberi, R. Azimirad, A. Z. Moshfegh and S. Rouhani, *J. Stat. Mech.*, 2006, **P09017**, 14.
- 33 R. Sivakumar, R. Gopalakrishnan, M. Jayachandran and C. Sanjeeviraja, *Optical Materials*, 2007, **29**, 687.
- 34 M. D. Antonik, J. E. Schneider, E. L. Wittman, K. Snow, J. F. Vetelino, and R. J. Lad, *Thin Solid Films*, 1995, **256**, 247.
- 35 H. S. Witham, P. Chindaudom, I. An, R.W. Collins, R. Messier, and K. Vedam, *J. Vac. Sci. Technol*A, 1993, **11**, 1881.
- 36 A. P. Giri and R. Messier, *Mater. Res. Soc. Symp. Proc.*, 1984, **24**, 221.
- 37 R. C. Ross, A. G. Johncock and A. R. Chan, *J. Non-Cryst. Solids*, 1984, **66**, 81.
- 38 W. C. D. Smith, *Displays*, 1982, **3**, 67.
- 39 S. A. Agnihotri, K. K. Saini and S. Chandra, *Ind. J. Pure Appl. Phys.*, 1986, **24**, 34.
- 40 K. Yamanaka, *Jpn. J. Appl. Phys.*, 1982, **25**, 1073.
- 41 P. Shen, N. Chi and K. Y. Chan, *J. Mater. Chem.*, 2000, **10**, 697.
- 42 S. H. Baeck, T. Jaramillo, G. D. Stucky and E. W. McFarland, *Nano Lett.*, 2002, **2**, 831.
- 43 H. M. A. Soliman, A. B. Kashyout, M. S. E. Nouby and A.M. Abosehly, *Int. J. Electrochem. Sci.*, 2012, **7**, 258.
- 44 W. L. Kwong, A. Nakaruk, P. Koshy and C. C. Sorrell, *J. Phys. Chem. C*, 2013, **117**, 17766.
- 45 W. L. Kwong, A. Nakaruk, P. Koshy and C. C. Sorrell, *Thin solid films*, 2013, **154**, 191.
- 46 N. Sharma, M. Deepa, P. Varshney and S. A. Agnihotry, *J. Sol-Gel Sci. Tec.*, 2000, **18**, 167.
- 47 N. Wang, J. Zhu, X. Zheng, F. Xiong, B. Huang, J. Shi and C. Li, *Faraday discuss.*, 2014, **176**, 185.
- 48 G. A. D. Wijs and R. A. D. Groot, *Phys. Rev. B: Condens. Matter*, 1999, **60**, 16463.
- 49 R. C. Lima, L. R. Macario, J. M. Espinosa, V. M. Longo, R. Erlo, N. L. Marana, J. R. Sambrano, M. L. Dos Santos, A. P. Moura, P. S. Pizani, J. Andres, E. Longo and J. A. Varela, *J. Phys. Chem. A*, 2008, **112**, 8970.
- 50 F. Zheng, M. Guo and M. Zhang, *CrystEngComm*, 2013, **15**, 277.
- 51 W. J. Lee, Y. K. Fang, J. Y. J. Ho, W. T. Hsieh, S. F. Ting, D. Huang, and F. C. Ho, *Journal of Electronic Materials*, 2000, **29**, 2.
- 52 X. H. Xia, J. P. Tu, J. Zhang, X. L. Wang, W. K. Zhang and H. Huang, *Sol. Energy Mater. Sol. Cells*, 2008, **92**, 628.
- 53 S. H. Kang, J. W. Lim, H. S. Kim, J. Y. Kim, Y. H. Chung and Y. E. Sung, *Chem. Mater.* 2009, **21**, 2777.
- 54 E. Barborini, P. Milani, C. Cepek, M. Sancrotti, *Adv. Mater.* 2005, **17**, 1842.
- 55 R. S. Vemuri, M. H. Engelhard and C.V. Ramana, *Appl. Mater. Interfaces*, 2012, **4**, 1371.
- 56 K. Senthil and K. Yong, *Nanotechnology*, 2007, **18**, 395604.
- 57 M. Li, M. Hu, D. Jia, S. Ma and W. Yan, *Sens. Actuators B*, 2013, **186**, 140.
- 58 R. Azimirad, N. Naseri, O. Akhavan and A. Z. Moshfegh, *J. Phys. D Appl. Phys.*, 2007, **40**, 1134.
- 59 X. H. Xia, J. P. Tu, J. Zhang, X. H. Huang, X. L. Wang, X. B. Zhao, *Electrochim. Acta*, 2010, **55**, 989.
- 60 G. F. Cai, X. L. Wang, D. Zhou, J. H. Zhang, Q. Q. Xiong, C. D. Gu and J. P. Tu, *RSC Adv.*, 2013, **3**, 6896.
- 61 J. Zhang, J. P. Tu, G. H. Du, Z. M. Dong, Y. S. Wu, L. Chang, D. Xie, G. F. Cai and X. L. Wang, *Sol. Energy Mater. Sol. Cells*, 2013, **114**, 31.
- 62 X. Liu, J. Zhao, Y. Cao, W. Li, Y. Sun, J. Lu, Y. Men and J. Hu, *RSC Adv.*, 2015, **5**, 47506.
- 63 R. R. Kharade, S. R. Mane, R. M. Mane, P. S. Patil and P. N. Bhosale, *J Sol-Gel Sci Technol*, 2010, **56**, 177.
- 64 N. Huo, S. Yang, Z. Wei and J. Li, *J. Mater. Chem. C*, 2013, **1**, 3999.
- 65 V. V. Kondalkar, S. S. Mali, R. R. Kharade, K. V. Khot, P. B. Patil, R. M. Mane, S. Choudhury, P. S. Patil, C. K. Hong, J. H. Kim and P. N. Bhosale, *Dalton Trans.*, 2015, **44**, 2788.
- 66 X. H. Xia, J. P. Tu, J. Zhang, J. Y. Xiang, X. L. Wang and X. B. Zhao, *Sol. Energy Mater. Sol. Cells*, 2010, **94**, 386.
- 67 S. R. Bathe and P. S. Patil, *Sol. Energy Mater. Sol. Cells*, 2007, **91**, 1097.
- 68 J. Zhang, J. P. Tu, X. H. Xia, Y. Qiao and Y. Lu, *Sol. Energy Mater. Sol. Cells*, 2009, **93**, 1840.
- 69 J. Zhang, J. P. Tu, X. H. Xia, X. L. Wang and C. D. Gu, *J. Mater. Chem.*, 2011, **21**, 5492.
- 70 A. Sangeeta and S. Debasish, *RCS Adv.*, 2014, **4**, 20145.
- 71 A. Sangeeta and S. Debasish, *Electrochim. Acta*, 2014, **138**, 115.
- 72 Z. H. Jiao, X. W. Sun, J. M. Wang, L. Ke and H. V. Demir, *J. Phys. D: Appl. Phys.*, 2010, **43**, 285501.
- 73 Z. H. Jiao, X. Wang, J. M. Wang, L. Ke, H. V. Demir, T. W. Koh and X. W. Sun, *Chem. Commun.*, 2012, **48**, 365.
- 74 S. H. Lee, R. Deshpande, P. A. Parilla, K. M. Jones, B. To, A. H. Mahan and A. C. Dillon, *Adv. Mater.*, 2006, **18**, 763.

## Journal Name

## ARTICLE

- 75 J. Zhang, X. L. Wang, X. H. Xia, C. D. Gu, Z. J. Zhao and J. P. Tu, *Electrochim. Acta*, 2010, **55**, 6953.
- 76 J. M. Wang, E. Khoo, P. S. Lee and J. Ma, *J. Phys. Chem. C*, 2009, **113**, 9655.